SURFACE DIFFUSION IN METAL EPITAXY - STRAIN EFFECTS

H. Brune, K. Bromann, and K. Kern

Institut de Physique Expérimentale, EPFL, CH-1015 Lausanne, Switzerland

ABSTRACT

A method is presented to measure both the barriers for intra- and interlayer diffusion for an epitaxial system with great accuracy. It is based upon the application of mean-field nucleation theory to variable temperature STM data. The validity and limits of applying nucleation theory to extract barriers for terrace diffusion are discussed in comparison to alternative methods like Kinetic Monte-Carlo (KMC) simulations. With this approach, a pronounced influence of strain on intra- and interlayer diffusion was established for Ag self diffusion on strained and unstrained Ag(111) surfaces. The strained surface was the pseudomorphic Ag monolayer on Pt(111) which is under 4.3% compressive strain. The barrier for terrace diffusion is observed to be substantially lower on the strained, compared to the unstrained Ag/Ag(111) case, 60±10 meV and 97±10 meV, respectively. A general method for the quantitative determination of the additional barrier for descending at steps is presented. It is based on the measurement of the nucleation rate on top of previously prepared adlayer islands as a function of island size and temperature. Application of this method reveals a considerable effect of strain also on interlayer diffusion. The additional barrier for interlayer diffusion decreases from 120±15 meV for Ag(111) homoepitaxy to only 30±5 meV for diffusion from the strained Ag layer down to the Pt(111) substrate. These examples illustrate the strong influence of strain on the intra- and interlayer mass transport which leads to a new concept of layer-dependent nucleation kinetics for heteroepitaxial systems. Finally, we discuss the relation between corner diffusion and island shapes. Low temperature aggregation on hexagonally close-packed metal surfaces generally is dominated by the microscopic difference between two edge orientations giving rise to anisotropic corner (and edge) diffusion. It is demonstrated how this anisotropy gives rise to dendritic island shapes with trigonal symmetry.

Surface Diffusion: Atomistic and Collective Processes
Edited by Michael C. Tringides, Plenum Press, New York, 1997

INTRODUCTION

There is great interest in understanding thin film growth on a fundamental level. The central atomic processes involved in epitaxial growth are mostly surface diffusion processes of single adatoms, comprising diffusion on terraces, over steps, and along edges. The first (intralayer diffusion) determines the mean free path of a diffusing adatom on terraces and on-top of islands which build up during deposition. It decides whether and how often an adatom can visit the island edge. The second (interlayer diffusion) is associated in general with an extra activation energy ΔE_S, adding to that for terrace diffusion.[1,2] This barrier describes the average number of attempts necessary for an adatom to descend the edge. It is the interplay of these two parameters that largely determines the film morphology. If atoms nucleate on-top of islands without having visited their edge at all, or after they have visited it too few times to descend, 3D growth occurs. Otherwise, the downward flux is high enough that the critical density for nucleation never builds up on-top of islands and the film grows 2D. However, also the third diffusion process (edge diffusion) can enter in determining the film morphology as it largely influences island shapes. For Pt(111) homoepitaxy, e.g., the absence of a certain step orientation in triangular islands is believed to be the reason for 3D growth at intermediate temperatures.[3]

In homoepitaxial systems, if no reconstructions are involved, both intra- and interlayer barriers remain unchanged with film thickness. In this case the mean free path of adatoms on-top of islands is comparable to the mutual island distance, which equals the maximum island size before coalescence. Hence, each atom visits the island edges at least once and the only parameter that determines the film morphology is the barrier for interlayer diffusion.

In heteroepitaxial systems, i.e., substrate and deposit consist of different species, strain effects due to the structural mismatch are important. The strain in the topmost layers, where nucleation occurs, changes with film thickness. Generally, it decreases with increasing number of layers, since the film adopts more and more at its bulk lattice constant as it grows thicker. Therefore, it is interesting to ask whether strain influences the nucleation kinetics and, if it does, how the growth scenario will be affected. We will show here for the case of Ag/Pt(111) that surface and interlayer diffusion can strongly alter from layer to layer due to different amounts of strain inherent in these layers. In fact, there have been several theoretical studies proposing strain should strongly alter surface diffusion and nucleation kinetics.[4-7] Only very recently, however, the influence of strain on nucleation kinetics could be examined experimentally.[8-11] We present experimental evidence for this effect observed for isotropic strain in metal epitaxy.

The method applied to measure surface migration barriers consists in the application of nucleation theory[12,13] to saturation island densities obtained from STM as a function of deposition temperature.[14,15] The analysis is done for a critical nucleus size of one, i.e., at temperatures where dimers are stable. In this case the activation energy (and attempt frequency) for surface migration can be determined directly, without requiring additional parameters like cluster binding energies.[14] The validity of this approach will be demonstrated in the first paragraph in comparison with KMC simulations. After this, it will be applied to study the influence of strain on terrace diffusion barriers. The additional barrier for interlayer diffusion can be measured by studying the nucleation probability on-top of preexistent islands as a function of their size[10,16] which will be illustrated in the third paragraph. Finally, we will discuss the influence of edge diffusion on island shapes for aggregation on hexagonally close-packed metal surfaces. It is demonstrated how a microscopic anisotropy in diffusion at the two types of edges, generally present on these surfaces, prevents the formation of classical diffusion limited aggregation (DLA) clusters and leads to dendritic island shapes with trigonal symmetry[17,18].

EXPERIMENT

The experiments were performed with a variable-temperature STM (25 K - 800 K) operating in UHV.[19] The Ag films on Pt(111) are prepared by deposition of Ag from an MBE Knudsen-cell at 450 K at a background pressure better than $2x10^{-10}$ mbar and subsequent annealing to 800 K. As a strained surface, we use the first Ag monolayer which grows pseudomorphically and is thus under 4.3% compressive strain.[20] To prepare an unstrained Ag(111) substrate we took advantage of the fact that very thick, annealed Ag films (>40 ML) grown on Pt(111) adopt the Ag(111) interplanar lattice constant and symmetry as characterized by He-diffraction.[21] STM images revealed that both the pseudomorphic Ag layer on Pt(111) and the Ag(111) surface consisted of extended flat terraces which were free of dislocations. For the study of nucleation kinetics, Ag submonolayer coverages have been deposited (flux $1.1x10^{-3}$ ML/s) onto these layers at various temperatures. Island densities are given in islands per Pt substrate atom. They were obtained on extended terraces to exclude the influence of steps and corrected for lateral drift.

RESULTS

Extracting Barriers for Terrace Diffusion from Island Densities

The classical method to quantitatively study diffusion on metal surfaces is field ion microscopy (FIM), where the motion of single atoms or clusters on single crystal facets of the FIM tip can be followed at low temperatures on the atomic level.[22,23] An alternative, although more indirect way to study diffusion, is to measure island densities that form upon deposition onto a single crystal surface as a function of temperature. The energy barrier to terrace diffusion is then commonly extracted by application of mean-field nucleation theory.[13] This method recently received considerable attention due to the fact that island densities became accessible in real space by the availability of scanning tunneling microscopy (STM). One of the first systematic STM studies of the variation of island densities with temperature was reported by Stroscio, Pierce, and Dragoset for Fe(100) homoepitaxy.[24] This study was performed for deposition above room temperature. Particularly for the case of close packed substrates, which reveal small energy barriers for diffusion and cluster dissociation, the observation of nucleation on terraces, respectively, the description of nucleation may become complicated at these temperatures by the large number of atomic processes involved. For example, assumptions need to be made about various cluster binding energies.[13] At cryogenic temperatures, on the other hand, diffusion is sufficiently slow to ensure nucleation on terraces without the influence of steps and, in addition, dimers are stable nuclei. This reduces a nucleation event to the encounter of two diffusing adatoms and allows for a direct, parameter-free analysis of surface diffusion barriers. It is, therefore, most convenient to study nucleation at low temperatures which can be achieved through the recent development of variable temperature STM.[25,26] With this technique, the initial stages of nucleation has been studied on the atomic level, yielding reliable and accurate barriers for surface diffusion on isotropic substrates.[9,14,27]

Since the method applied here to study surface diffusion relies on the application of mean-field nucleation theory, we discuss experiments of Ag nucleation on Pt(111) that allow for a direct test of certain predictions from nucleation theory. We subsequently show that an analysis of the energy barrier and attempt frequency for surface diffusion from nucleation theory is fully consistent with results from KMC simulations; both describe the experimental island densities quite well.

One of the central predictions of mean-field nucleation theory, frequently applied for the analysis island densities, is that the saturation density of all stable clusters n_x depends upon the deposition flux F and the adatom diffusion D as follows (for the most relevant case in metal epitaxy, i.e., complete condensation, and 2D islands)

$$n_x \propto \left(\frac{D}{F}\right)^{-\chi} \exp\left(\frac{E_i}{(i+2)kT}\right). \quad (1)$$

The exponent χ in the first term on the right-hand side of Eq. (1) is $\chi = i/(i+2)$, where i is the critical cluster size. A critical nucleus is an island that becomes stable upon attachment of a monomer. Here, stable refers to the time scale of submonolayer deposition, where a stable island grows more likely than it decays. The Boltzmann term contains the total binding energy E_i of the critical cluster, which, in a simple bond counting model, equals the number of lateral bonds times their bond energy E_b. The critical nucleus size can be inferred from investigation of the flux dependence of the island density through Eq. (1). From its temperature dependence, the parameters for surface diffusion and cluster binding energies can then be extracted in a second step.

To get insight into the regimes of nucleation from an experimental point of view, we follow the evolution of the submonolayer film morphology with increasing coverage for Ag deposition onto a Pt(111) surface held at 75K. Four STM images taken isothermal to deposition are shown in Fig. 1. The very initial stages of nucleation are depicted in Figs. 1a and 1b. The islands, detectable as bright spots, predominantly constitute dimers and trimers. The mean island size, as obtained from the coverage divided by the density, is 2.4±0.4 atoms and 2.6±0.5 atoms, for the STM images shown in Figs. 1a and 1b, respectively. This is exactly the value expected from nucleation involving dimers as stable nuclei. In the course of deposition, dimers form until they reach a density similar to that of the diffusing monomers. At that point, these monomers partly migrate towards each other creating new nuclei (dimers), and partly attach to existing dimers thereby creating trimers. The result is a mixture of mostly dimers and trimers giving rise to the mean island size of about 2.5 atoms. The fact that the mean size did not change from Fig. 1a to 1b, although the coverage had been increased by a factor of about three, is characteristic for the so-called pure nucleation regime, since additional deposition predominantly results in the formation of new nuclei. Increasing the coverage further by a factor of 5 leads to the transition from nucleation to growth. In the STM image in Fig. 1c, the density is increased by a factor of two, accompanied by a considerable increase in the average island size to 6±1 atoms. Further increase of the coverage by a factor of two leads exclusively to island growth (12±2 atoms per island in Fig. 1d). Thus, Fig. 1d shows the pure growth regime, where the island density has saturated, i.e., it is large enough that each arriving atom has sufficient mobility to reach an existing island with a higher probability than to hit a second mobile adatom and form a new nucleus.

The set of STM images shown in Fig. 1 completely characterizes nucleation of Ag/Pt(111) at 75 K, as it yields the saturation island density as well as the stable nucleus size at this temperature. At higher temperatures, however, direct observation of the mean island size to determine the critical nucleus size is less practical since the pure nucleation regime is then restricted to extremely low coverages. There are various other ways to get information on the critical island size at a certain temperature. One way to detect up to which temperature, e.g., dimers are stable, is to measure the temperature threshold for the onset of Ostwald ripening.[28] For this purpose a large number density of dimers (and also trimers) is produced upon deposition at low temperature, and the island density is monitored by STM as a function of annealing temperature. At the onset of dimer dissociation (or dimer diffusion),

the island density suddenly decreases, due to the dissociation of smaller islands in favor of larger ones, i.e., due to Ostwald ripening. For Ag/Pt(111), the threshold for dimer dissociation for annealing periods of half an hour is 100 K, which implies that on the much shorter time scale of deposition, the Ag dimer is stable on Pt(111) up to 110 K.

It is important to notice, this method to deduce the stable nucleus size does not rely on nucleation theory. Therefore, it supplies additional information that can serve to independently test, e.g., the flux dependence predicted from this theory. For Ag/Pt it is found indeed that island densities vary as $F^{1/3}$ for 80 and 110 K in agreement with Eq. (1).[29] The island size distributions,[29] as well as a change in slope in the Arrhenius behavior of the island densities observed at 110 K[14] (not shown here), all are fully consistent with the fact that dimers are the stable nuclei up to 110 K and show the agreement between nucleation theory and experiment.

The saturation island density directly reflects the adatom mobility, therefore it is expected to follow the Arrhenius law. Measured saturation island densities for Ag/Pt at a coverage of 0.12 ML are shown in Arrhenius representation in Fig. 2a in comparison with mean-field calculations. From the experimental data it can be seen that there is a linear regime for temperatures from 110 K down to about 75 K followed by a downward bending of the island densities measured for lower temperatures. The linear regime reflects the expected power law for D/F from Eq. (1), while the downward bending to lower island densities is due to the fact that for lower temperatures, diffusion becomes slow with respect to deposition (at $D/F < 10^5$) leading to a certain density of monomers left after deposition. These monomers then either nucleate new islands or attach to existing ones after deposition has

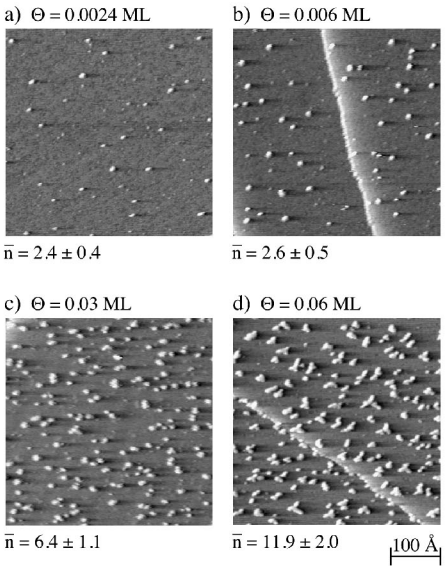

Figure 1. Four STM images showing the evolution of the island density, size and shape with increasing coverage for Ag deposition ($F = 1.1 \times 10^{-3}$ ML/s) onto Pt(111) at 75 K. Coverages and mean island sizes are indicated.

been terminated. This nucleation regime is called post-nucleation; it is characterized by monotonically decreasing island size distributions, and has been described in detail for Cu/Ni(100).[30] Square lattices generally reveal higher migration barriers, therefore post-nucleation effects are expected for an extended temperature range on these substrates.

The solid line in Fig. 2a shows the best fit to the experimental data by mean-field rate equations which have been solved self-consistently.[29,31] Taking into account for post-nucleation, the rate equations have been integrated until all monomers were gone, which starts to play a role for T < 75 K. The fact, that even at 50 K apparently all monomers are gone when the island density is measured with STM, is not expected from the diffusion rate at this temperature and the time between deposition and STM experiment. It is presumably due to the interaction of the STM tip with adsorbed monomers. The influence of the STM tip has been shown to considerably decrease the diffusion barrier for Pt/Pt(111).[27] Therefore, in our example, the few remaining monomers are probably attaching to existing islands due to the measurement itself. This does not obscure the results since stable nuclei turn out to be unaffected by the measurement.

The mean-field calculation shows excellent agreement with experiment, it has been performed with a migration barrier of E_m = 168 meV and an attempt frequency of ν_0 = 6.76×10^{13} s^{-1} (notice, that $D = \frac{1}{3} \nu_0 \exp(-E_m/kT)$ since hopping has been assumed to take place from fcc to fcc sites). A self-consistent solution to the mean-field rate equations such as shown in Fig. 2a is mathematically demanding.[31] It is therefore valuable to discuss alternative ways to extract parameters for surface diffusion from the type of data shown in Fig. 2a.

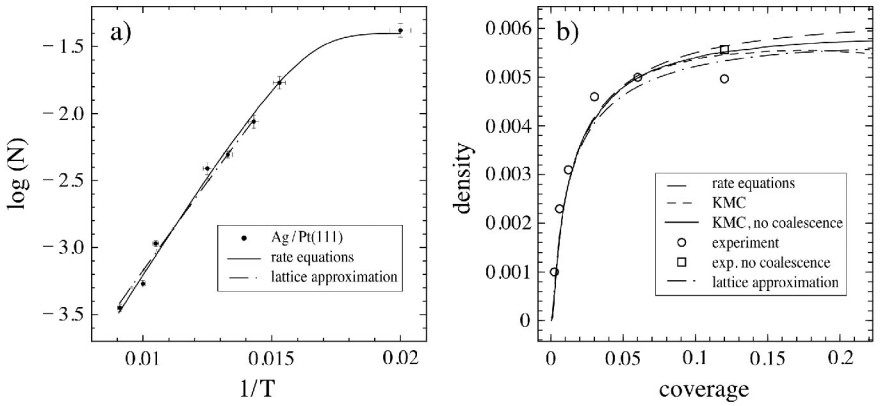

Figure 2. Comparison of experimental island densities for Ag/Pt(111) to calculations from self-consistent and approximate solutions of mean-field nucleation theory and KMC simulations. a) Arrhenius plot of saturation island densities (Θ = 0.12 ML) for the regime where dimers are stable nuclei. b) Island density versus coverage at 75 K.

The most easy and widely used approach is to apply Eq. (1) to the linear part in the Arrhenius plot, where dimers are stable (i = 1) and extract the migration barrier and the attempt frequency from the slope of the linear regression to the data and its intersection with the ordinate. This far more simpler approach yields fairly good agreement with the values obtained from the full analysis. Taking the STM data for 75 K ≤ T ≤ 110 K, where $1 \times 10^5 \leq D/F \leq 4 \times 10^8$, one obtains E_m = 170±10 meV and $\nu_0 = 4 \times 10^{13.0 \pm 0.5}$ s^{-1}. (For the attempt frequency, the proportionality factor in Eq. (1) has been set to $\eta(\Theta)$ = 0.2. This value has

been given by Venables, see curve for i = 1 at $\Theta \approx 0.1$ ML in Fig. 6c of ref.,[13] and is also obtained in the self-consistent analysis by Bales). Notice, however, that great care must be taken when selecting the data attributed to the linear regime. As can be seen from inspection of Fig. 2a, the calculated curve starts to bend for T < 75 K, respectively, $D/F < 1x10^5$. Therefore, we emphasize that only data for $D/F > 1x10^5$ should be analyzed in a linear regression. Thus, a slightly lower barrier of $E_m = 157\pm10$ meV ($\nu_0 = 6x10^{13.0\pm0.8}$ s^{-1}) has been obtained when the slope was analyzed including data down to 65 K,[14] where it is seen from Fig. 2a that post-nucleation already decreases island densities.

The evolution of the island density with coverage for our example of Ag/Pt(111) at 75 K is plotted in Fig. 2b (compare STM images in Fig. 1). Again, there is perfect agreement with the self-consistent rate equation analysis. Since the analysis did not account for coalescence, an experimental value at 0.12 ML for the (hypothetical) island density without coalescence has been derived, which can be accomplished, since coalesced islands are discerned by their shape from those that grew from a single nucleus. Figure 2b also shows KMC simulations performed on a square lattice with the same parameters as in the rate equations. They are fully in accordance with experiment and rate theory. The results from KMC simulations performed on a hexagonal lattice taking account for the dendritic island shape[29] are hardly distinguished from the KMC results shown here. In general, KMC simulations have served as a valuable test for nucleation and scaling theories.[31-35] For our example of Ag/Pt, Fig. 2b shows that the self-consistent rate equations are in quantitative agreement with these simulations and both perfectly describe the experiment.

Another approach is to integrate rate equations of nucleation within certain approximations for the capture numbers σ reducing the calculational effort significantly.[14,27] These approximations can now be compared to the exact solutions and KMC simulations discussed above. The capture numbers describe the capability of islands or monomers to capture diffusing adatoms. They generally involve solutions of two-dimensional diffusion problems. This is not the case in the geometrical concept[36] where capture numbers are equal to the island diameter seen by the approaching monomers. This concept, when applied to fractal islands, yields $\sigma_x = 2+x^{1/1.7}$ (with x being the island size in atoms, the constant of 2 accounts for atoms diffusing towards sites adjacent to the island perimeter).[14] This approximation has successfully been applied to calculate the evolution of island densities with coverage at a single temperature.[14] It has been shown, however, to be inconsistent in so far as it yields a higher slope in the Arrhenius representation of the island densities compared to the slope expected from Eq. (1)[27]. It was noted earlier that the geometric concept gives even more inaccurate predictions than constant capture rates,[37] which should therefore be preferred as the most simple approximation. A more elaborate approach is obtained from solving the diffusion equation in the lattice approximation.[12,37] This yields an analytic expression for σ_x (stable islands) that depends only upon coverage. For monomers, on the other hand, a constant value of $\sigma_1 = 3$ corresponding to the geometrical concept can be used for simplicity.

In summary, the straight forward analysis of island densities within mean-field nucleation theory by means of Eq. (1), when performed for $D/F > 10^5$ and a critical nucleus size of one, allows the determination of the energy barriers and attempt frequencies for surface diffusion with sufficient accuracy. This precision can further be increased when comparing experimental data either to self-consistent mean-field theory or to KMC simulations, which both are fully consistent with each other. In addition, nucleation theory has recently been subject to direct experimental tests which underline its validity for isotropic substrates. This has placed its application for extracting parameters for surface diffusion from island densities on isotropic substrates on a firm basis. For anisotropic substrates, the description is more complicated since terrace diffusion, edge diffusion, and sticking to islands may be anisotropic. These effects are difficult to discern. For strongly anisotropic diffusion, as the case on fcc(110) surfaces, a mean-field rate equation treatment was put

forward[38] and applied to estimate diffusion barriers.[39] For nucleation on weakly anisotropic systems, like fcc(100)-hex reconstructed substrates,[40,41] as well as generally for island size and distance distributions, comparison of experimental data to KMC simulations may be more appropriate.

Strain and Terrace Diffusion

A strong layer dependence of island densities becomes evident from inspection of Fig. 3. It shows nucleation on the Pt(111) substrate (a), the first Ag layer adsorbed on Pt(111) (b), as well as on Ag(111) (c). The structure of the first Ag layer is pseudomorphic with respect to the Pt(111) substrate.[20,42-44] The Ag interatomic distance in this layer is reduced therefore by 4.3% with respect to the Ag bulk value. The Ag(111) surface has been prepared by deposition of a thick Ag film onto Pt(111) at 450 K and subsequent annealing to 800 K. This yields extended, perfectly flat terraces, giving rise to a single diffraction peak in high-resolution He-diffraction measurements which corresponds to the interplanar lattice constant of bulk Ag(111) of 2.89 Å.[45] The island density on these surfaces shows an oscillatory behavior with layer thickness. It decreases strongly when going from the Pt substrate to the pseudomorphic first Ag layer and then slightly increases again for nucleation on Ag(111).

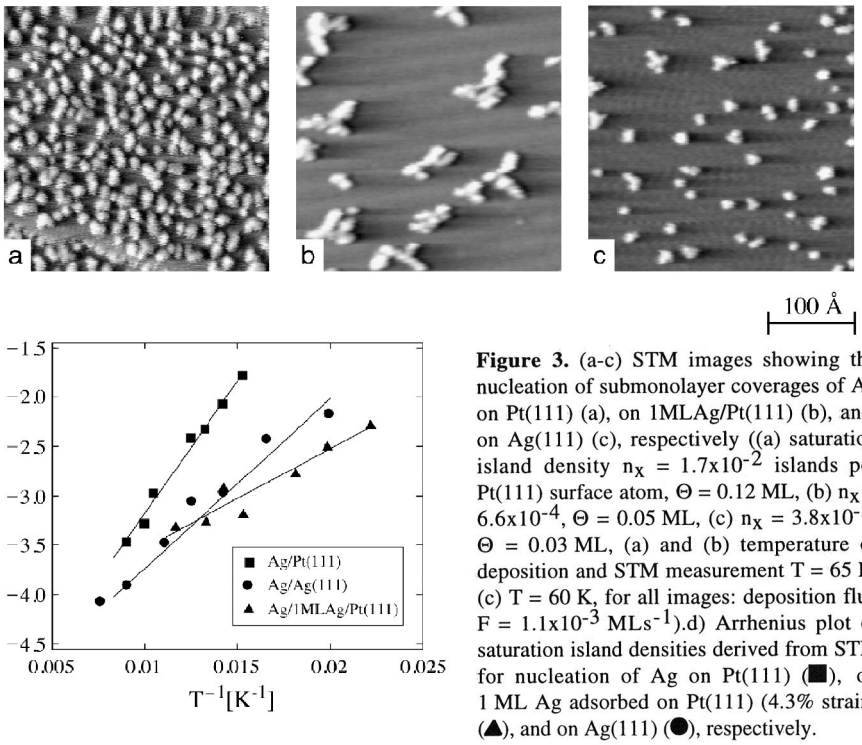

Figure 3. (a-c) STM images showing the nucleation of submonolayer coverages of Ag on Pt(111) (a), on 1MLAg/Pt(111) (b), and, on Ag(111) (c), respectively ((a) saturation island density $n_X = 1.7 \times 10^{-2}$ islands per Pt(111) surface atom, $\Theta = 0.12$ ML, (b) $n_X = 6.6 \times 10^{-4}$, $\Theta = 0.05$ ML, (c) $n_X = 3.8 \times 10^{-3}$, $\Theta = 0.03$ ML, (a) and (b) temperature of deposition and STM measurement T = 65 K, (c) T = 60 K, for all images: deposition flux $F = 1.1 \times 10^{-3}$ MLs^{-1}).d) Arrhenius plot of saturation island densities derived from STM for nucleation of Ag on Pt(111) (■), on 1 ML Ag adsorbed on Pt(111) (4.3% strain) (▲), and on Ag(111) (●), respectively.

To quantify the parameters for surface diffusion of Ag on these layers, we measured the saturation island density as a function of temperature for the three cases shown in Fig. 3a-c. The results are shown in Arrhenius representation in Fig. 3d. The temperature dependence of saturation island densities (Θ = 0.12 ML) on these three substrates shows strongly differing slopes, indicative for differing migration barriers. Nucleation on the pseudomorphic Ag layer is characterized by the smallest slope, followed by Ag(111) and finally by Pt(111). These slopes directly yield the parameters for surface diffusion on these layers since, for the data shown here, dimers are stable. This is indicated by the absence of bends in the Arrhenius in Fig. 3d and has also been verified by dimer annealing experiments. The resulting migration barriers E_m on these different isotropic layers amount to 168±10 meV for Ag/Pt (see preceding section), 60±10 meV for the pseudomorphic Ag layer and finally 97±10 meV for Ag diffusion on a strain-free Ag(111) surface.[9]

The lowering of the surface migration barrier by 40% on the pseudomorphic Ag layer with respect to that on Ag(111) is remarkable. It is difficult to decide *a-priori* whether strain or the electronic adlayer-substrate coupling is causing this effect. We have recently studied the influence of lattice strain and electronic adlayer-substrate coupling for the Ag/Pt(111) system by calculations with effective medium theory (EMT).[46,47] In these calculations, strain effects clearly dominate the electronic adlayer-substrate coupling. Actually, it turned out the electronic coupling weakened the effect, as the diffusion barrier for a by 4.3% compressed Ag-slab was found to be even lower than that of the pseudomorphic monolayer on Pt(111). The change in diffusion barrier, evident from Fig. 3, can thus clearly be attributed to strain.

Rather good absolute values for migration barriers on close-packed surfaces have recently been provided by ab-initio (LDA) calculations. The barrier for Ag/Pt(111) has been calculated by Feibelman to 200 meV[48] in reasonably good, and recently by Ratsch and Scheffler to 150 meV[49] in quite good, agreement with our experimental value; that for Pt(111) self-diffusion to 380 meV,[50] which overestimates the established experimental value of 250±20 meV.[27,50] For Ag(111) self-diffusion, 100 meV has been obtained by K. Jacobsen et al. with ab-initio calculations with generalized gradient correction (GGA)[51] in agreement with the value of 90 meV obtained by Ratsch and Scheffler.[49] Also, these theoretical values are in remarkable coincidence with experiment (97±10 meV, see above). Therefore, it is particularly valuable that these more precise calculations are in agreement with the interpretation formerly deduced from EMT calculations.[9] Ratsch and Scheffler find reduced diffusion barriers on the pseudomorphic Ag layer on Pt(111), 65 meV, as well as on a compressively strained (by 4.3%) Ag(111) slab, also 65 meV.[49] These values agree well with the experiment and fully support the interpretation that strain is the origin for the decrease in the diffusion barrier (40%) on a compressively strained Ag layer (4.3%) when compared to strain free Ag(111).

In the light of these results for isotropic strain and terrace diffusion nucleation on anisotropic surfaces can be understood in terms of strain effects. The anisotropy of diffusion observed for nucleation on hex reconstructed fcc(100) surfaces[40,41] might be understood in terms of an anisotropic strain resulting from the superposition of a hexagonal on a square lattice. Also for nucleation on lattices which have dislocations and therefore also anisotropic strain, a strong effect on island densities has been established. For Ni nucleation on the dislocation network and moiré structures formed by Ni on Ru(0001) a strong layer dependence of island densities has been observed.[8]

For nucleation of Ag on a regular array of dislocations, formed by the second Ag layer on Pt(111),[20,43] the island density has been found to be strongly increased with respect to the unstrained and the homogeneously strained case discussed above.[9] The fact that only few of the nuclei form directly on dislocations is indicative for these dislocations to represent a rather effective repulsive barrier for adatoms that confines them to the pseudomorphic

domains. At 110 K, the island density reaches a value, where on the average one island forms per unit cell of the dislocation network. This situation is characterized by almost equally spaced and sized islands. In general, the influence of anisotropic strain on nucleation can be employed to significantly decrease the width of island size and distance distributions when compared to nucleation on isotropic substrates. Here, one takes advantage of the fact there is generally a strong repulsive interaction between dislocations leading to their arrangement in periodic patterns. This periodicity is then reflected in regular island spacing. Since island spacing distributions are directly correlated to island size distributions,[52] the latter are significantly more narrow than for nucleation on a homogeneous substrate.

Strain and the Interlayer Diffusion

The barriers for interlayer diffusion have been measured based upon the following idea which was first put forward by Tersoff et al..[16] Application of mean-field nucleation theory to calculate the nucleation probability on-top of an island yields a sharp transition from 0 to 1 at a critical island radius which depends upon temperature. This can be exploited to extract the additional barrier for interlayer diffusion, ΔE_S, and its attempt frequency from a series of measurements of the nucleation probability on-top of preexistent islands as function of their size and of the substrate temperature at which the post-deposition is performed.[10] Islands with defined sizes can be prepared by two-dimensional Ostwald ripening, i.e., annealing of small islands until the mean island size has reached the desired value.[28] Figure 4a) shows an example where 0.1 ML Ag have been deposited at 40 K onto Pt(111) which predominantly leads to dimers. Afterwards, this surface was annealed to 230 K, which yielded compact islands of a mean size of 200 atoms. The island size distribution from Ostwald ripening is more narrow than that for nucleation, however, it is still sufficiently broad to study the transition of second layer nucleation as a function of island radius.

Figure 4b) shows, after a second deposition, there are small original islands where no nucleation occurs on-top and larger ones where nucleation always occurs. This behavior has been studied quantitatively for three temperatures for Ag homoepitaxy and Ag nucleation on

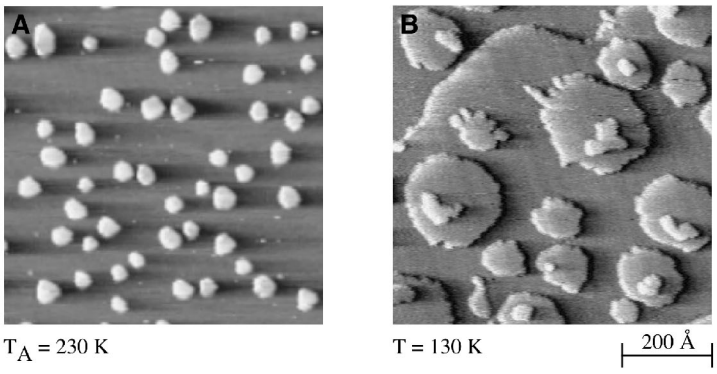

Figure 4. (a) STM image illustrating the formation of 2D Ag islands on Pt(111) with defined sizes via deposition of 0.1 ML Ag at 40 K and subsequent annealing to 230 K (2D-Ostwald ripening). (b) STM image showing the result of the subsequent nucleation experiment, in which 0.1 ML Ag are deposited ($F = 1.1 \times 10^{-3}$ ML/s) at 130 K on islands that were previously grown via Ostwald ripening on Ag(111).

strained Ag islands adsorbed on Pt(111). Since the barriers and attempt frequencies for surface diffusion are known for both cases, the only fit parameters are those for interlayer diffusion. An additional barrier of ΔE_s = 120±15 meV and attempt frequency of ν_s = $1x10^{13\pm1}$ s^{-1} are obtained for the interlayer diffusion in Ag homoepitaxy. Therefore, an adatom must overcome more than twice the barrier for terrace diffusion in order to descend the steps. This explains the fact that Ag(111) homoepitaxy is three-dimensional at temperatures below 400 K.[53] In a recent analysis of the occupancy of open layers as a function of coverage, developed for homoepitaxy, Meyer et al.[8] found ΔE_s = 150±20 meV for Ag/Ag(111) from experiments at 300 K, which is in fair agreement with our result.

In contrast, the activation energy for step-down diffusion in the heteroepitaxial system Ag/Ag-islands/Pt(111) is determined to ΔE_s = 30±5 meV (ν_s = $1x10^{9\pm1}$ s^{-1}). This is a rather small barrier which can easily be overcome. This is the reason for the perfect 2D growth of the first Ag monolayer on Pt(111) down to temperatures as low as 80 K. The influence of island shape, i.e., whether they are compact or ramified, is less important, since even on large compact islands produced from Ostwald ripening, all Ag atoms post-deposited at 80 K are observed to descend.

The strained pseudomorphic Ag islands on Pt(111) preferentially relieve their strain at the edges where the Ag atoms are more free to expand. This might cause a lowering in lateral binding energy of atoms at the island edge which, in turn, facilitates exchange processes. It is known that for several fcc (111) substrates, exchange is, at least at B-steps (see Figure 5c), the dominant mechanism by which interlayer diffusion takes place.[3,54] A second major difference to the homoepitaxial case is the different binding energy for an Ag adatom on the Pt(111) surface. While in homoepitaxy obviously both upper and lower terrace have the same binding energies, they are generally different in heteroepitaxy. For the case of Ag/Pt(111), the binding energy of a Ag atom on the first Ag layer is about 170 meV less than that on the Pt terrace below, as inferred from thermal desorption experiments.[42] This potential energy difference as well as strain relaxation at the edge, discussed above, are possible reasons for the small additional step-edge barrier of the strained case compared to Ag(111).

Edge Diffusion and Island Shapes

Island shapes generally contain information on edge diffusion. It is known that island growth at low temperatures can lead to branching caused by the reduced mobility of adatoms at the island edges. In the absence of edge diffusion, ramification takes place into random directions as in Diffusion Limited Aggregation (DLA) scenarios.[55,56] For square lattices edge diffusion is generally found to be associated with a low barrier compared to terrace diffusion, leading to compact island shapes on these surfaces.[57] On close-packed substrates, on the other hand, edge diffusion was thought to have a high barrier and low temperature metal epitaxy was expected to be the realization of DLA.

The STM image reproduced in Fig. 5a, and other examples in literature,[17,18,58] clearly demonstrate that the branches grow into three preferred directions (the crystallographic $\langle\bar{1}\,\bar{1}\,2\rangle$-directions), leading to Y-shapes for small islands (see Fig. 1d) and to dendrites with a triangular envelope for larger ones (Fig. 5a).

The atomic process responsible for dendritic growth was recently found to be the asymmetry in diffusion of atoms from 1-fold corner sites towards one of the two non-equivalent steps present on a hexagonal surface.[18,58] These two step-orientations differ in structure, the A-type steps are {100} facets, and B-step are {111}-facets (see heptamer in Fig. 5c).

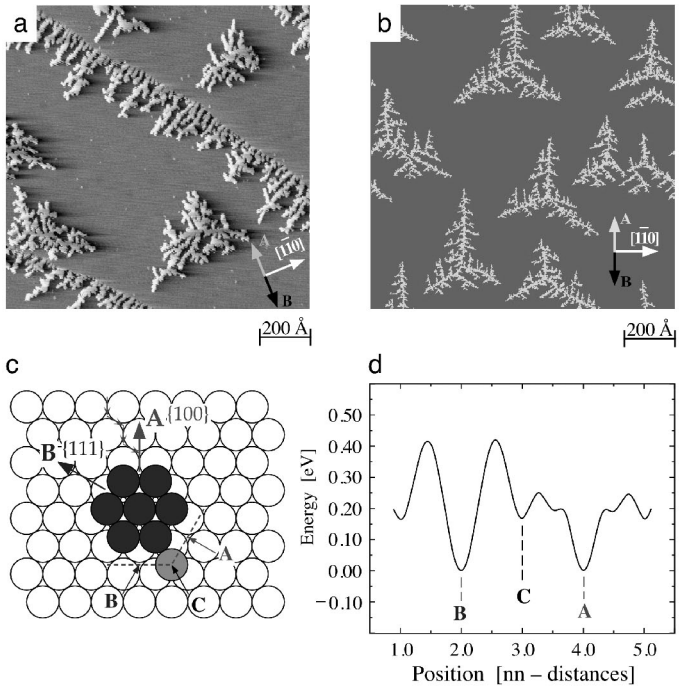

Figure 5. a) STM image showing dendritic growth for Ag/Pt(111) at 120K (Θ = 0.12 ML). b) KMC simulation with anisotropic corner diffusion as the central mechanism giving rise to dendritic growth (parameters see Table 1). c) Heptamer on a hexagonal lattice with its two non-equivalent step orientations and d) difference in total energy for diffusion around it calculated with EMT for Ag/Pt(111).

For Ag/Pt(111) and Ag/Ag(111), EMT calculations show that diffusion towards A-steps is activated as soon as terrace diffusion sets in, since it requires a comparable energy barrier, whereas diffusion towards B-steps is inhibited (see Figure 5d and Table 1). This asymmetry can be rationalized from simple geometric reasons. From inspection of the model in Fig. 5c, it becomes evident that displacement from a corner to an A-step can be done via an hcp-hollow site without loosing the coordination to the heptamer, whereas for diffusion towards a B-step the hcp-site is situated too close towards the island. Thus, the adatom must walk almost over an on-top site, which requires a higher activation energy. This asymmetry in diffusion from corners to the two step types leads to preferred population of A-steps and to branching perpendicular to these steps. This can be verified by KMC simulations shown in Fig. 5b which nicely reproduce the experiment in Fig. 5a (the barriers applied for this simulation are listed in Table 1).

The anisotropy in population of A- and B-steps generally characterizes close-packed substrates which implies that dendritic growth is the rule rather than the exception on these lattices. Which step orientation is the preferred one can be different from system to system. The sign of the strain is expected to play a decisive role, since it determines which diffusion path is more favorable along the island edge.

Table 1. Energy barriers for the most relevant atomic diffusion processes involved in metal aggregation on hexagonal substrates for the systems serving as example in this article (E_m stands for terrace diffusion, ΔE_s for the additional barrier for interlayer diffusion, E_{Ac} for corner-to-A-step, E_{Bc} for corner-to-B-step, E_{Ae} and E_{Be} denote A- and B-edge diffusion). * E_m has been lowered in order to account for the lower island density due to dimer dissociation setting in at 120 K.

Ag diffusion on substrates:	E_m STM	ΔE_s STM	E_m EMT	E_{Ac}/E_{Bc} EMT	E_{Ae}/E_{Be} EMT	E_{Ac}/E_{Bc} KMC	E_m KMC
Pt(111)	168±10	—	80	80/248	187/389	160/500	120*
Ag(111)	97±10	120±15	67	73/139	222/300	—	—
1MLAg/Pt(111)	60±10	30±5	50	39/165	167/354	—	—

CONCLUSIONS

We applied mean-field nucleation theory to variable temperature STM data to measure the energy barriers and attempt frequencies for intra- and interlayer diffusion for Ag homoepitaxy and heteroepitaxy on the (111) surfaces of Ag and Pt. On the pseudomorphic Ag layer, the barrier for terrace diffusion is lowered by 40% with respect to that on Ag(111). Similarly, the additional barrier for interlayer diffusion is substantially lower on the pseudomorphic layer compared to Ag(111) homoepitaxy. The effect seen for intralayer diffusion can unequivocally be attributed to the 4.3% compressive strain present in the pseudomorphic Ag layer on Pt(111). The low interlayer barrier for the strained system is likely to be also an effect of strain which may facilitate exchange processes.

While it has been demonstrated for a particular model system that misfit strain can strongly alter barriers for intra- and interlayer diffusion, its implications for heteroepitaxial growth in the kinetic regime are of general significance. This implies a new concept of layer-dependent adatom mobilities and island densities caused by strain which constitutes, together with the barrier for intralayer diffusion, an essential ingredient for the understanding and modeling of the kinetics of heteroepitaxial growth.

We presented STM experiments for aggregation of Ag/Pt(111) showing dendritic growth with branches growing into preferred directions from lowest temperatures onward. It was shown how this island shape can been correlated to edge diffusion. The mechanism giving rise to this trigonal symmetry was identified by using EMT energy calculations and kinetic Monte-Carlo simulations. The key process is the preferential diffusion of atoms from one-fold corner sites towards A-steps. This significantly increases the adatom diffusion towards these steps and thereby promotes dendritic growth. The mechanism explains all experimental observations for low temperature metal aggregation on hexagonally close-packed substrates and suggests that dendritic growth, rather than randomly branched fractals is the rule for aggregation on these surfaces.

ACKNOWLEDGMENT

We gratefully acknowledge valuable contributions of H. Röder, C. Boragno, and G. S. Bales during various stages of this work. We also acknowledge collaboration with J. Jacobsen, K. W. Jacobsen, P. Stoltze, and J. Nørskov in performing simulations with Effective Medium Theory and kinetic Monte-Carlo.

REFERENCES

1. G. Ehrlich and F. G. Hudda, *J. Chem. Phys.* **44**, 1039 (1966).
2. R. L. Schwoebel and E. J. Shipsey, *J. Appl. Phys.* **37**, 3682 (1966).
3. J. Jacobsen, K. W. Jacobsen, P. Stoltze, and J. K. Nørskov, *Phys. Rev. Lett.* **74**, 2295 (1995).
4. S. V. Ghaisas, *Surf. Sci.* **223**, 441 (1989).
5. C. Roland and G. H. Gilmer, *Phys. Rev. B* **46**, 13428 (1992).
6. C. Ratsch and A. Zangwill, *Appl. Phys. Lett.* **63**, 2348 (1993).
7. H. Spjut and D. A. Faux, *Surf. Sci.* **306**, 233 (1994).
8. J. A. Meyer, P. Schmid, and R. J. Behm, *Phys. Rev. Lett.* **74**, 3864 (1995).
9. H. Brune, K. Bromann, H. Röder, K. Kern, J. Jacobsen, P. Stolze, K. Jacobsen, and J. Nørskov, *Phys. Rev. B* **52**, R14380 (1995).
10. K. Bromann, H. Brune, H. Röder, and K. Kern, *Phys. Rev. Lett.* **75**, 677 (1995).
11. H. Röder, K. Bromann, H. Brune, and K. Kern, *Surf. Sci.* submitted (1996).
12. J. A. Venables, *Philos. Mag.* **17**, 697 (1973).
13. J. A. Venables, G. D. T. Spiller, and M. Hanbücken, *Rep. Prog. Phys.* **47**, 399 (1984).
14. H. Brune, H. Röder, C. Boragno, and K. Kern, *Phys. Rev. Lett.* **73**, 1955 (1994).
15. J. A. Stroscio and D. T. Pierce, *Phys. Rev. B* **49**, 8522 (1994).
16. J. Tersoff, A. W. D. v. d. Gon, and R. M. Tromp, *Phys. Rev. Lett.* **72**, 266 (1994).
17. H. Brune, C. Romainczyk, H. Röder, and K. Kern, *Nature* **369**, 469 (1994).
18. H. Brune, K. Bromann, J. Jacobsen, K. Jacobsen, P. Stoltze, J. Nørskov, and K. Kern, *Surf. Sci. Lett.* **349**, L115 (1996).
19. H. Brune, H. Röder, C. Romainczyk, C. Boragno, and K. Kern, *Appl. Phys. A* **60**, 167 (1995).
20. H. Brune, H. Röder, C. Boragno, and K. Kern, *Phys. Rev. B* **49**, 2997 (1994).
21. C. Romainczyk, M. Krzyzowski, P. Zeppenfeld, G. Comsa, and K. Kern, to be published.
22. G. Ehrlich, *Surf. Sci.* **246**, 1 (1991).
23. G. L. Kellogg, *Surf. Sci. Rep.* **21**, 1 (1994).
24. J. A. Stroscio, D. T. Pierce, and R. A. Dragoset, *Phys. Rev. Lett.* **70**, 3615 (1993).
25. M. Bott, T. Michely, and G. Comsa, *Surf. Sci.* **272**, 161 (1992).
26. H. Röder, H. Brune, J. P. Bucher, and K. Kern, *Surf. Sci.* **298**, 121 (1993).
27. M. Bott, M. Hohage, M. Morgenstern, T. Michely, and G. Comsa, *Phys. Rev. Lett.* **76**, 1304 (1995).
28. H. Röder, E. Hahn, H. Brune, J. P. Bucher, and K. Kern, *Nature* **366**, 141 (1993).
29. H. Brune, S. Bales, J. Jacobsen, C. Boragno, and K. Kern, to be published .
30. B. Müller, B. Fischer, L. Nedelmann, H. Brune, and K. Kern, *Phys. Rev. B* submitted (1996).
31. G. S. Bales and D. C. Chrzan, *Phys. Rev. B* **50**, 6057 (1994).
32. M. C. Bartelt and J. W. Evans, *Phys. Rev. B* **46**, 12675 (1992).
33. D. E. Wolf, in *Scale Invariance, Interfaces, and Non-Equilibrium Dynamics*, vol. M. Droz, K. J. McKane, J. Vannimenus, and D. E. Wolf, Eds., Plenum, New York, (1994), p 1.
34. J. G. Amar, F. Family, and P. M. Lam, *Phys. Rev. B* **50**, 8781 (1994).
35. J. G. Amar and F. Family, *Phys. Rev. Lett.* **74**, 2066 (1995).
36. G. Zinsmeister, *Thin Solid Films* **7**, 51 (1971).
37. M. J. Stowell, *Phil. Mag.* **26**, 349 (1972).

38. J. W. Evans and M. C. Bartelt, *J. Vac. Sci. Technol.* **A 12**, 1800 (1994).
39. J. P. Bucher, E. Hahn, P. Fernandez, C. Massobrio, and K. Kern, *Europhys. Lett.* **27**, 473 (1994).
40. S. Günther, E. Kopatzki, M. C. Bartelt, J. W. Evans, and R. J. Behm, *Phys. Rev. Lett.* **73**, 553 (1994).
41. T. R. Linderoth, J. J. Mortensen, K. W. Jacobsen, E. Laegsgaard, I. Stensgaard, and F. Besenbacher, *Phys. Rev. Lett.* **77**, 87 (1996).
42. T. Härtel, U. Strüber, and J. Küppers, *Thin Sol. Films* **229**, 163 (1993).
43. G. Rangelov, T. Fauster, U. Strüber, and J. Küppers, *Surf. Sci.* (Proc. ECOSS-14) **331-333**, 948 (1995).
44. Notice, the first monolayer of Ag on Pt(111) grows only pseudomorphic when either completed or present as small islands. When the islands reach a certain size the formation of dislocations is observed. Interestingly, these dislocations disappear again upon completion of the first layer.
45. C. Romainczyk, Ph. D. Thesis, Ecole Polytechnique Fédérale de Lausanne, (1994).
46. K. W. Jacobsen, J. K. Nørskov, and M. J. Puska, *Phys. Rev. B* **35**, 7423 (1987).
47. P. Stoltze, *J. Phys. Condens. Matter* **6**, 9495 (1994).
48. P. J. Feibelman, *Surf. Sci.* **313**, L801 (1994).
49. C. Ratsch and M. Scheffler (private communication).
50. P. J. Feibelman, J. S. Nelson, and G. L. Kellogg, *Phys. Rev. B* **49**, 10548 (1994).
51. J. J. Mortensen, B. Hammer, O. H. Nielsen, K. W. Jacobsen and J. K. Nørskov, in *Solid State Sciences Series*, vol. 121, A. Okiji, Eds. (Springer, 1996).
52. P. A. Mulheran and J. A. Blackman, *Phil. Mag. Lett.* **72**, 55 (1995).
53. H. A. v. d. Vegt, H. M. v. Pinxteren, M. Lohmeier, E. Vlieg, and J. M. Thornton, *Phys. Rev. Lett.* **68**, 3335 (1992).
54. S. C. Wang and G. Ehrlich, *Phys. Rev. Lett.* **75**, 2964 (1995).
55. T. A. Witten and L. M. Sander, *Phys. Rev. Lett.* **47**, 1400 (1981).
56. T. A. Witten and L. M. Sander, *Phys. Rev. B* **27**, 5686 (1983).
57. Z. Zhang, X. Chen, and M. G. Lagally, *Phys. Rev. Lett.* **73**, 1829 (1994).
58. M. Hohage, M. Bott, M. Morgenstern, Z. Zhang, T. Michely, and G. Comsa, *Phys. Rev. Lett.* **76**, 2366 (1995).